

# Subwavelength imaging from a multilayered structure containing interleaved nonspherical metal-dielectric composites

Lihong Shi<sup>1,2</sup> and Lei Gao<sup>1,\*</sup>

<sup>1</sup>*Jiangsu Key Laboratory of Thin Films, Department of Physics, Suzhou University, Suzhou 215006, People's Republic of China*  
<sup>2</sup>*Department of Physics and Centre for Computational Science and Engineering, National University of Singapore, Singapore 117542, Republic of Singapore*

(Received 29 October 2007; revised manuscript received 19 April 2008; published 27 May 2008)

A thin multilayered structure with interleaved nonspherical metal-dielectric composites slices and dielectric slices may be modeled as the metamaterial with anisotropic permittivity. The signs of diagonal elements of the permittivity tensor can be controlled by the particles' shape, the volume fraction of metal particles, and the incidental wavelengths. To one's interest, when the spheroidal nanoparticles are oblate in shape, the wavelength range in which components of the permittivity have different signs is widened, and the magnitude of optical absorption band becomes weak. Since both physical anisotropy and low absorption are helpful for improving the subwavelength image resolution, the multilayered structure containing metal-dielectric composite layer of nonspherical particles may be designed as a superlens device. In addition, the incident wavelength and the number of nanolayers are found to play crucial roles in enhancing the evanescent field performance too.

DOI: [10.1103/PhysRevB.77.195121](https://doi.org/10.1103/PhysRevB.77.195121)

PACS number(s): 78.20.Ci, 42.25.Dd, 68.37.Uv, 77.22.Ej

## I. INTRODUCTION

Conventional optical lenses based on ordinary positive materials are not able to overcome the standard diffraction limit, since the evanescent waves carrying the subwavelength details of the source exponentially decay in free space. However, for a planar slab of metamaterials with the refractive index being  $-1$ ,<sup>1</sup> both propagating and evanescent waves contribute to the resolution of the image, hence, attaining perfect resolution. Later, Pendry's "perfect lens" was shown not to exist for realistic dispersive and lossy materials.<sup>2</sup> In spite of this, numerical simulations showed that a slab of silver as a lens can create images with subwavelength resolution by the amplification of evanescent field within the slab via the surface plasmons.<sup>1</sup> The proposal was further verified by experimental results,<sup>3,4</sup> which demonstrated the reality of subwavelength imaging using silver slabs in optical frequency range.

Recently, multilayered structures containing alternating layers of metal and dielectrics attract much attention due to the improvement of subwavelength image performance relative to a single slab.<sup>5-11</sup> The mechanisms for the realizations of superlens were generally different. For instance, the multilayered structures in Refs. 5 and 6 were found to be helpful to reduce the effect of absorption, resulting in better image resolution in the near-field zone. A transmission device formed by a periodic metal-dielectric layered structure was demonstrated to possess subwavelength imaging based on the canalization mechanism, i.e., without involving negative refraction and amplification of evanescent modes.<sup>7</sup> Later, in the same structure, the Fabry-Pérot resonance effect was also utilized to improve the subwavelength imaging quality.<sup>8</sup> Furthermore, for structures with much thinner metal and dielectric layers,<sup>9,10,12</sup> the effective medium concept was important to determine the subwavelength imaging performance. Through tuning the permittivities or the thicknesses of individual layers, one obtained  $\text{Re}(\epsilon_{ex}) > 0$  and  $\text{Re}(\epsilon_{ez})$

$< 0$  from the homogenization theory, where  $\epsilon_e$  is the effective permittivity tensor for the whole structure. It was further shown that the selection of low-loss materials and suitable incident wavelength has a significant impact on the subwavelength image performance. In this paper, we shall study the optical properties of a multilayered structure containing alternating nanolayers of metal-dielectric composites and dielectrics. For metal-dielectric layers, both metal and dielectric nanoparticles are assumed to be nonspherical in shape.<sup>13</sup> In this connection, the introduction of the particles' shape provides an alternative freedom to tune the anisotropic optical properties of the structure, and hence, may be useful for the improvement of subwavelength imaging performance.<sup>14</sup> Similar as in Refs. 7, 9, 10, and 15, we may regard this multilayered structure as a homogeneous effective metamaterial with anisotropic dielectric permittivity under the quasistatic approximation. The metamaterial with anisotropic property may translate the high-frequency wave vector values from evanescent modes to propagating modes, and focus these modes to form a subwavelength image.<sup>16</sup> Through tuning the nanoparticles' shape, it is possible to change two components of the effective permittivity tensor and reduce the absorption in the metamaterials. As a consequence, the subwavelength image performance will be found to be strongly dependent on the nanoparticles' shape, the incident wavelength, and so on.

The paper is organized as follows. In Sec. II, we describe the model for the multilayered structure containing nanolayers of metal-dielectric composite and dielectrics, and establish our theory. In Sec. III, the dependence of subwavelength image performance on the particles' shape, the incidental wavelength, and nanolayer numbers is investigated. In Sec. IV, we summarize our conclusions and discussions.

## II. THEORETICAL DEVELOPMENT

We consider a multilayered structure composed of alternating metal-dielectric composite nanolayers and dielectric

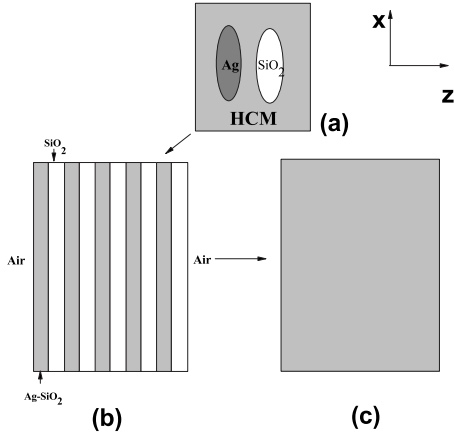


FIG. 1. Schematic for the multilayered structure composed of alternating Ag-SiO<sub>2</sub> composites layer and SiO<sub>2</sub> dielectric layer.

nanolayers, as shown in Fig. 1. For the composite layer, spheroidal metal particles of permittivity  $\epsilon_m$ , volume fraction  $p$ , and spheroidal dielectric particles (of permittivity  $\epsilon_d$  and volume fraction  $1-p$ ) are randomly distributed. Without loss of generality, we assume both metal and dielectric particles to be nonmagnetic with permeability  $\mu=1$ . In order to achieve the physical anisotropy, all nanoparticles in the composite layer are identically aligned with the principal axes parallel to the  $z$  axis. With all length scales much less than the incident wavelength, one can take a two-step approach to investigate the effective permittivity tensor of the multilayered structure.<sup>17,18</sup>

In the first step, one homogenizes the metal-dielectric layer as a slab with the equivalent permittivity tensor  $\vec{\epsilon}_1$ . When an external electric field ( $\mathbf{E}_0$ ) is applied to the metal-dielectric layer, the local field ( $\mathbf{E}$ ) is written as an integral equation<sup>19</sup>

$$\delta\vec{\epsilon}(\mathbf{r}) \cdot \mathbf{E}(\mathbf{r}) = \delta\vec{\epsilon}(\mathbf{r}) \cdot \mathbf{E}_0 + \delta\vec{\epsilon}(\mathbf{r}) \cdot \int d\mathbf{r}' \vec{g}(\mathbf{r}, \mathbf{r}') \cdot \delta\vec{\epsilon}(\mathbf{r}') \cdot \mathbf{E}(\mathbf{r}'), \quad (1)$$

where  $\delta\vec{\epsilon}(\mathbf{r}) = \delta\vec{\epsilon}(\mathbf{r}) - \delta\vec{\epsilon}_1$  and  $\vec{g}(\mathbf{r}, \mathbf{r}')$  is the second-derivative tensor of the Green function  $G(\mathbf{r}, \mathbf{r}')$ .

Under the condition that net polarization for the composite layer goes to zero, it was shown that Eq. (1) can be decoupled by the self-consistent equation<sup>19-21</sup>

$$\langle (\vec{I} - \vec{\Gamma} \delta\vec{\epsilon}_1)^{-1} \delta\vec{\epsilon}_1 \rangle = 0, \quad (2)$$

where  $\vec{I}$  is a  $3 \times 3$  unit tensor and  $\delta\vec{\epsilon}_1 = \epsilon_i - \vec{\epsilon}_1$  ( $i=m,d$ ). The tensor  $\vec{\Gamma}$  defined by a surface integral is readily evaluated as follows:<sup>13,22,23</sup>

$$\vec{\Gamma} = -\vec{L}(\vec{\epsilon}_1)^{-1}, \quad (3)$$

where  $\vec{L}$  is a depolarization tensor. For simplicity, all nanoparticles are assumed to be rotationally spheroidal in shape with the principal axes being the axes of the spheroids. In this connection,  $\vec{L}$  is diagonal with components  $L_x=L_y=(1-L_z)/2$  and  $L_z$ , i.e.,

$$\vec{L} = \begin{pmatrix} (1-L_z)/2 & 0 & 0 \\ 0 & (1-L_z)/2 & 0 \\ 0 & 0 & L_z \end{pmatrix}. \quad (4)$$

In Eq. (4),  $L_z$  is a geometry-dependent quantity given by<sup>20,24</sup>

$$L_z = \frac{1}{1-r^2} + \frac{r}{(r^2-1)^{3/2}} \ln(r + \sqrt{r^2-1}) \quad (5)$$

for prolate spheroids with an aspect ratio  $r=c/a > 1$ , and

$$L_z = \frac{1}{1-r^2} - \frac{r}{(1-r^2)^{3/2}} \arccos r \quad (6)$$

for oblate spheroids with  $r=c/a < 1$ , where  $a$  ( $=b$ ) and  $c$  are, respectively, radii of a spheroid along three Cartesian axes. Note that  $L_z=1/3$  for a spherical particle,  $L_z \rightarrow 0$  for a needlelike particle, and  $L_z \rightarrow 1$  for a platelike particle.

By substituting Eqs. (3) and (4) into Eq. (2), one yields

$$\vec{\epsilon}_1 = \begin{pmatrix} \epsilon_{1x} & 0 & 0 \\ 0 & \epsilon_{1y} & 0 \\ 0 & 0 & \epsilon_{1z} \end{pmatrix}, \quad (7)$$

where  $\epsilon_{1x}$  ( $=\epsilon_{1y}$ ) and  $\epsilon_{1z}$  are the three components of the equivalent permittivity of the composite layer, which are simplified as<sup>22,23</sup>

$$p \frac{\epsilon_m - \epsilon_{1j}}{\epsilon_{1j} + L_j(\epsilon_m - \epsilon_{1j})} + (1-p) \frac{\epsilon_d - \epsilon_{1j}}{\epsilon_{1j} + L_j(\epsilon_d - \epsilon_{1j})} = 0, \quad j=x,y,z, \quad (8)$$

and its solution admits

$$\epsilon_{1j} = \frac{1}{2(L_j-1)} \left\{ -\epsilon_m(p-L_j) - \epsilon_d(1-p-L_j) \pm \sqrt{[\epsilon_m(p-L_j) + \epsilon_d(1-p-L_j)]^2 - 4L_j(L_j-1)\epsilon_m\epsilon_d} \right\}. \quad (9)$$

As adopted in Refs. 22–25, we assume that the depolarization tensor  $\vec{L}$  is independent of the equivalent permittivity tensor for the composite nanolayer. In other words, we do not take into account the effect of dielectric anisotropy on the depolarization factors. Actually, for a rigorous treatment, one may resort to Refs. 24 and 26–29. Qualitatively, the consideration of the anisotropic property tends to minimize the eccentricity of the spheroid, and thereby weakens the physical anisotropy of the composite layers.<sup>24</sup>

In the second step, we estimate the effective permittivity tensor of the whole multilayered structures  $\vec{\epsilon}_e$  with the form<sup>7,9,10,30</sup>

$$\vec{\epsilon}_e = \begin{pmatrix} \epsilon_{ex} & 0 & 0 \\ 0 & \epsilon_{ey} & 0 \\ 0 & 0 & \epsilon_{ez} \end{pmatrix}, \quad (10)$$

where its diagonal components are determined by

$$\epsilon_{ex} = \epsilon_{ey} = \epsilon_1 f_1 + \epsilon_2 f_2, \quad \text{and} \quad \epsilon_{ez} = \frac{1}{f_1/\epsilon_{1z} + f_2/\epsilon_2}, \quad (11)$$

where  $f_1(=d_1/d)$  and  $f_2(=d_2/d)$  ( $d=d_1+d_2$ ) are the ratios of two layer thicknesses, and  $\epsilon_2$  is the permittivity of dielectric layer. It is evident that the multilayered structure is uniaxially dielectric, and the uniaxial anisotropy leads to the negative refraction.<sup>31</sup> Incidentally, Yannopoulos *et al.*<sup>32</sup> considered the metamaterials with negative refractive index consisting of the polaritonic and plasmonic spheres. The polaritonic resonance is responsible for the existence for negative effective permeability, while the plasmonic resonance is responsible for negative effective permittivity. In this connection, the metamaterials can exhibit negative refractive index because of both negative permittivity and negative permeability, and the subwavelength image resolution in such metamaterials is due to the near-field amplification.<sup>33</sup>

Under present circumstances, the electric and magnetic responses of materials are decoupled. Since the structure is nonmagnetic ( $\mu=1$ ), we take a two-dimensional light beam of transverse magnetic polarization with its wave vector in  $x$ - $z$  plane only. The dispersive relation for these waves is given by

$$\frac{k_x^2}{\epsilon_{ez}} + \frac{k_{ez}^2}{\epsilon_{ex}} = \left(\frac{\omega}{c}\right)^2 = \left(\frac{2\pi}{\lambda}\right)^2 = k_0^2. \quad (12)$$

From Eq. (12), it is easy to find that when both  $\epsilon_{ex}$  and  $\epsilon_{ez}$  are positive ( $\epsilon_{ex} \neq \epsilon_{ez}$ ), the relationship between  $k_x$  and  $k_{ez}$  is elliptic. In this case,  $k_{ez}$  is real for small  $k_x$ , indicating the propagating waves, and  $k_{ez}$  is imaginary for large  $k_x$ , corresponding to the evanescent waves. However, when  $\epsilon_{ex}$  and  $\epsilon_{ez}$  have opposite signs, one yields (i)  $\epsilon_{ex} > 0$ ,  $\epsilon_{ez} < 0$  and (ii)  $\epsilon_{ex} < 0$ ,  $\epsilon_{ez} > 0$ . For the former case,  $k_{ez}$  is always real for any  $k_x$  and all frequency components are propagating. On the other hand, for the latter, the high-spatial frequency components with large  $k_x$ , which would normally be evanescent in the free space, correspond to propagating waves now. Therefore, in these two cases, subwavelength details (with large  $k_x$ ) can be delivered to the imaging plane through the multilayered structure, and good subwavelength imaging may be obtained. Although our analysis is valid for real permittivity without loss, the lossy case can be qualitatively understood in a similar way.<sup>10,16</sup>

Here, we would like to mention that because the metal-dielectric composites slab is anisotropic, the high-spatial frequency components with large  $k_x$ , which would normally be evanescent, may propagate in such anisotropic composites when  $\epsilon_{ex}$  and  $\epsilon_{ez}$  possess opposite signs,<sup>5,10,16</sup> resulting in subwavelength image resolution. However, for previous composite films of nonspherical shape,<sup>14</sup> since the particles are randomly oriented, the equivalent permittivity is isotropic in essence. For subwavelength imaging, the equivalent permittivity should be equal to negative permittivity of the surrounding medium. Therefore, the near field components are evanescent in the composites slab, but may be amplified due to the excitation of surface plasmon at the interface.

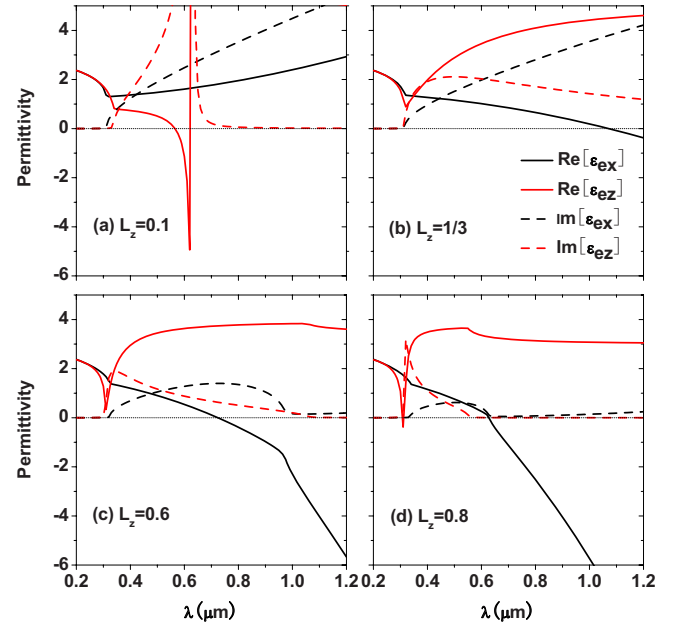


FIG. 2. (Color online) The effective dielectric permittivity such as  $\text{Re}(\epsilon_{ex})$  (black solid lines),  $\text{Im}(\epsilon_{ex})$  (black dashed lines),  $\text{Re}(\epsilon_{ez})$  (red solid lines), and  $\text{Im}(\epsilon_{ez})$  (red dashed lines) as a function of the incident wavelength  $\lambda$  for the metal volume fraction  $p=0.4$ .

### III. NUMERICAL RESULTS

We are now in a position to perform numerical calculations. We consider the multilayered structures containing alternating nanolayers of Ag-SiO<sub>2</sub> and SiO<sub>2</sub>. The permittivity of silver is given by the Drude model,<sup>14,15,34</sup>

$$\epsilon_m = \epsilon'_m + i\epsilon''_m = \epsilon_0 - \frac{\omega_p^2}{\omega(\omega + i\Gamma)}, \quad (13)$$

where  $\epsilon_0$  is the contribution due to interband transitions ( $\epsilon_0=5$ ),  $\omega_p$  is the bulk plasma frequency ( $\omega_p=9$  eV), and  $\Gamma$  is the relaxation constant ( $\Gamma=0.02$  eV). In what follows, we only consider the case that  $d_1=d_2$ . As a result, the metal volume fraction  $p$  and the depolarization factor  $L_z$  are the key factors to control the signs of the components of  $\vec{\epsilon}_e$ . In addition, to avoid the nonlocal dispersion,<sup>35,36</sup> we do not consider the extreme case such as  $L_z \rightarrow 0$  and  $L_z \rightarrow 1$ , and only aim at those for finite spheroidal particles with intermediate oblate or prolate shape.

Figure 2 shows the real (solid lines) and imaginary parts (dashed lines) of the effective permittivity for a Ag-SiO<sub>2</sub> composites and SiO<sub>2</sub> multilayered structure as a function of the incident wavelength  $\lambda$ . For the four graphs, there is always one region where  $\text{Re}(\epsilon_{ex})$  and  $\text{Re}(\epsilon_{ez})$  take the opposite signs. For instance, for  $L_z=0.1$  (prolate particles), one can find that  $\text{Re}(\epsilon_{ex})$  is positive, while  $\text{Re}(\epsilon_{ez})$  is negative in the wavelength region around  $0.56 \mu\text{m}$ , as shown in Fig. 2(a). For the other three graphs, the inverse case is obtained, that is,  $\text{Re}(\epsilon_{ex}) < 0$  and  $\text{Re}(\epsilon_{ez}) > 0$ . As we showed before, the metamaterials with such anisotropy can translate the high-frequency wave vector values from evanescence to propagating. With the increase in the depolarization factor, the wavelength range, where  $\text{Re}(\epsilon_{ex})$  and  $\text{Re}(\epsilon_{ez})$  take the opposite

signs, is widened. In detail, for  $L_z=1/3$  (spherical nanoparticles), the wavelength regime is around 1.08-1.2  $\mu\text{m}$ ; and for  $L_z=0.6$  (oblate nanoparticles with small deviation from the spherical one), a range from 0.75 to 1.2  $\mu\text{m}$  is found, obviously wider than the one for  $L_z=1/3$ . To one's interest, for  $L_z=0.8$  (oblate particles with large deviation from the spherical shape), one can obtain a wavelength range of 0.63-1.2  $\mu\text{m}$ , which covers a longer part of the visible spectrum. Furthermore, it is found that the imaginary part of the effective dielectric permittivity exhibits a broad surface-plasmon absorption band due to the electromagnetic interactions between individual grains. The effect of absorption is known to be deleterious for the image transfer.<sup>5</sup> For spherical particles, the absorption band is wide and the magnitude in the band is large. Interestingly, when nanoparticles in composite layer are oblate spheroidal in shape, the absorption band becomes narrower, and the corresponding magnitude is much lower than the one for spherical case. Therefore, the adjustment of the particles' shape may result in tunable physical anisotropy and low dielectric absorption, and thereby improve subwavelength image resolution. However, since each composite layer is thin, the size of metal particles along  $z$  axis should not be large. As a consequence, we shall aim at the oblate case, in which  $\text{Re}(\epsilon_{ex}) < 0$  and  $\text{Re}(\epsilon_{ez}) > 0$ .

The subwavelength imaging lies in the enhanced transmission of the high-spatial frequencies of the source field. For a multilayered structure with the total thickness  $d$ , the plane wave transmission coefficient is

$$T(k_x) = \frac{4\epsilon_{ex}\epsilon_0k_{ez}k_{0z}}{(\epsilon_{ex}k_{0z} + \epsilon_0k_{ez})^2 e^{-ik_{ez}d} - (\epsilon_{ex}k_{0z} - \epsilon_0k_{ez})^2 e^{ik_{ez}d}}, \quad (14)$$

where  $k_{0z} = \sqrt{k_0^2\epsilon_0 - k_x^2}$  and  $k_{ez} = \sqrt{k_0^2\epsilon_{ex} - k_x^2\epsilon_{ex}/\epsilon_{ez}}$  are the  $z$  components of wave vectors in the free space with the permittivity  $\epsilon_0$  and the effective medium, respectively.

Figure 3 shows the transmission spectra for various depolarization factors with  $\lambda=800$  nm [Fig. 3(a)] and incidental wavelengths with  $L_z=0.6$  [Fig. 3(b)]. In Fig. 3(a), for  $L_z=1/3$  (green dotted lines), both components of the effective permittivity are positive [see Fig. 2(b)]. As a result, the transmission coefficient is close to unity for small wave vectors, but it sharply drops for large  $k_x$ , corresponding to evanescent waves. For  $L_z=0.6$  (red dashed lines), since the components of the effective permittivity take the opposite signs [ $\text{Re}(\epsilon_{ex}) < 0$  and  $\text{Re}(\epsilon_{ez}) > 0$ ], one would expect large range of  $k_x$  for which  $T$  is almost unity. However, this is not the case due to large dielectric losses for  $L_z=0.6$ . Even so, the exponential decaying rate for large  $k_x$  is still less rapid than that of  $L_z=1/3$ . To one's interest, peculiar oscillatory behavior appears for  $L_z=0.8$  (black solid lines). In detail, the transmission coefficient has a series of peaks, decreasing in magnitude. For the first resonant peak, the wave is nonpropagating inside the system due to the imaginary  $k_z$ , and hence the resonance results from the coupled surface plasmons located on the surface of the system. On the other hand, for the resonant peaks for higher wave vectors, the wave is propagating due to  $\text{Re}(\epsilon_{ex}) < 0$  and  $\text{Re}(\epsilon_{ez}) > 0$  with small losses [see Fig. 2(d)], and the resonant peaks corre-

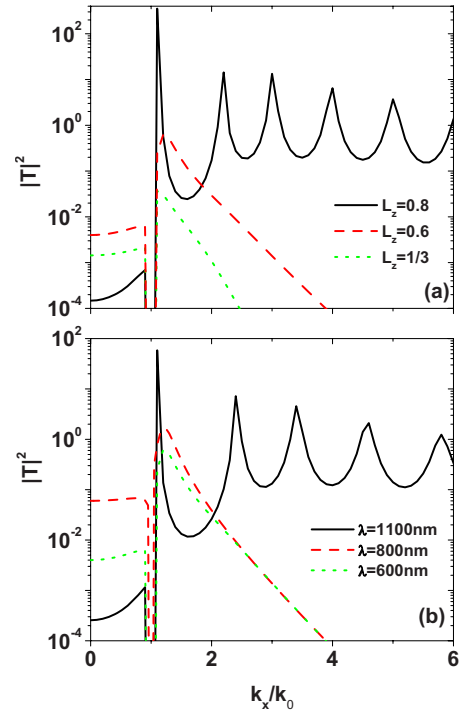


FIG. 3. (Color online) The transmission spectra as a function of normalized wave vector  $k_x/k_0$ . (a)  $\lambda=800$  nm, and  $L_z=0.8$  (black solid lines), 0.6 (red dashed lines), 1/3 (green dotted lines); (b)  $L_z=0.6$ , and  $\lambda=1100$  nm (black solid lines), 800 nm (red dashed lines), 600 nm (green dotted lines). The total thickness of the structure  $d$  is set to be 400 nm.

spond to Fabry-Pérot resonances-standing waves inside the system.<sup>10</sup> Therefore, good subwavelength imaging resolution should be found for  $L_z=0.8$ .

Figure 3(b) shows the influence of the incidental wavelengths on the optical transmission of the multilayered structure with the depolarization factor  $L_z=0.6$ . As evident from the figure, the transmission spectrum varies with the incidental wavelengths. For the incident wavelength  $\lambda=600$  nm (green dotted lines), both components of the effective per-

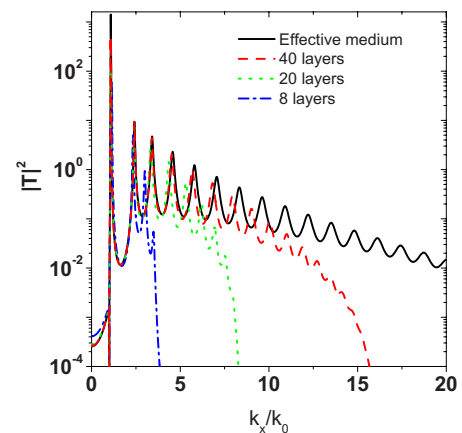


FIG. 4. (Color online) The transmission spectra for effective medium case (black solid lines),  $n=40$  (red dashed lines),  $n=20$  (green dotted lines), and  $n=8$  (blue dashed-dotted lines). The relevant parameters are  $L_z=0.6$ ,  $\lambda=1100$  nm, and  $d=400$  nm.

mittivity are positive, and no evanescent waves performance accordingly exists. However, for  $\lambda=1100$  nm (black solid lines) (in the near-infrared frequency range), one observes a broad transmission spectrum with a series of resonant peaks even for large transverse wave vectors  $k_x$ . The broad transmission spectrum for large  $k_x$  results from that the wave is still able to propagate in the composite nanolayers, and shows good evanescent field performance clearly.

It is known that in order to obtain a better subwavelength image resolution, one may increase the number of layers, while keeping the total length of the multilayered structure fixed.<sup>5</sup> Figure 4 shows the influence of the number of layers  $N$  on the transmission spectra for the total length  $d=400$  nm. We find that when the transmission coefficient  $T$  drops to  $1 \times 10^{-4}$ , the cutoff transverse wave vector  $k_x$  is

increased and the subwavelength image resolution is improved with the increase in  $N$  or the decrease in each layer width.<sup>9</sup> Therefore, to obtain good evanescent field performance, the layers should be thinner, for which the effective medium theory can describe the system well.<sup>10</sup>

In what follows, we further investigate the effects of the particles' shape and the incidental wavelength on the subwavelength imaging. In this connection, we shall consider the image of an infinitely thin line source, lying along the  $y$  axis. The metamaterial slab consisting of the multilayered structure is placed next to the line source. If we neglect the radiations reflected from the structure, which will generate the additional currents, we can estimate the  $x$  component of the transmitted field as<sup>10</sup>

$$E_x^{TM} = \int_{-\infty}^{\infty} \int_{-\infty}^{\infty} e^{ik_x x + ik_y y + ik_{0z}(z-d) - i\omega t} T(\sqrt{k_x^2 + k_y^2}, \omega) \frac{E_0(k_y) k_x^2}{k_x^2 + k_y^2} dk_x dk_y. \quad (15)$$

For a line source, because it is uniform in strength and infinitely long, one yields  $E_0(k_y) \propto \delta(k_y)$ . Then, Eq. (15) can be simplified as

$$E_x^{TM} = \frac{E_0}{k_0} \int_{-\infty}^{\infty} \frac{4\epsilon_{ex}\epsilon_0 k_{ez} k_{0z} e^{ik_x x + ik_{0z}(z-d) - i\omega t}}{(\epsilon_{ex} k_{0z} + \epsilon_0 k_{ez})^2 e^{-ik_{ez} d} - (\epsilon_{ex} k_{0z} - \epsilon_0 k_{ez})^2 e^{ik_{ez} d}} dk_x. \quad (16)$$

In Fig. 5, we plot the intensity of the transmitted field for various depolarization factors and incidental wavelengths as a function of  $k_0 x$ . In Fig. 5(a), we note that the intensity  $|E_x|^2$  for  $L_z=0.8$  (black solid lines) is amplified with respect to the cases for  $L_z=0.6$  (red dashed lines) and  $L_z=1/3$  (green dotted lines). In addition, for  $L_z=0.8$ , the sharp image peak of the line source is clearly observed, and the full width at half maximum for  $|E_x|^2$  ( $\sim 0.043\lambda$ ) is considerably smaller than  $0.7\lambda$  for  $L_z=0.6$ . This suggests a subwavelength imaging operation of the multilayered structure containing oblate spheroidal particles. On the contrary, for  $L_z=1/3$  (the spherical shape), the intensity of  $|E_x|^2$  has a very low value and almost approaches zero, so that the resolution is not referred here. In Fig. 5(b), both the positions of the image peaks and the imaging quality are found to be variant with the change in incident wavelengths, as expected. For  $\lambda=1100$  nm (black solid lines), the sharp image peak appears at about  $k_0 x=2.3$ , and an approximate subwavelength resolution of about  $0.043\lambda$  is achieved. However, for the other two cases, the intensities of the transmitted field  $|E_x|^2$  have very low values, and thus a poor imaging performance. Therefore, we make a conclusion that the subwavelength imaging is strongly dependent on both the particles' shape and the incident wavelength.

In the end, we examine the effect of the layer width on the subwavelength imaging, by calculating the transmitted field intensity. Figure 6 shows the transmitted electric field intensity, plotted as a function of  $k_0 x$  for various different layer numbers. The position of the peaks is found to be propor-

tional to the layer width. As the layers get thinner, the image peak goes sharper, and thereby the better subwavelength resolution may be achieved.

#### IV. CONCLUSION

We have studied the "multilayered superlens," composed of alternating layers of the metal-dielectric nanocomposites and dielectric materials. This class of "superlens" can translate the evanescent (near-field) waves to propagating waves under the condition that two components of the effective permittivity take the opposite signs. In our model, such a condition can be realized by tuning either the shape of metallic particles or the incident wavelengths. We further show that when the nanoparticles of composite layer are oblate spheroidal in shape, the region, in which the components of effective permittivity take opposite signs, becomes wide, and the corresponding absorption is low. As a consequence, one expects that the subwavelength image resolution can be improved through tuning the nanoparticles' shape. This is numerically demonstrated by our calculations of both the transmission spectra and the image of the line source.

Here, we would like to add a few comments. We show that when the layers get thinner, the subwavelength imaging is better, for which effective medium theory describes well. As one knows, effective medium theory is valid when inhomogeneities are much smaller than the wavelength in both parallel and normal directions.<sup>15</sup> To obtain an appreciable

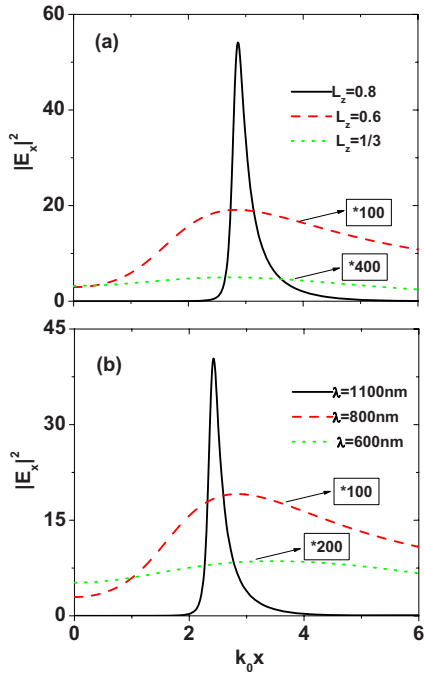


FIG. 5. (Color online) The transmitted field intensity for a line source for (a)  $L_z=0.8$  (black solid lines), 0.6 (red dashed lines), and 1/3 (green dotted lines); (b)  $\lambda=1100$  nm (black solid lines), 800 nm (red dashed lines), and 600 nm (green dotted lines). The distance from the image plane to the multilayered structure is 10 nm.

subwavelength resolution, the size of metal-dielectric composites is required to be about ten to several ten nanometers. With the development of nanotechnology, the fabrication for such metal-dielectric composites is fully achievable.<sup>7,15</sup> On the other hand, effective medium theory has its limitations, as pointed out in Ref. 37. Since no exact theory exists at present, effective medium theory can still be used as a first step to estimate the permittivity of the nanocomposites. Actually, for better subwavelength imaging of the multilayered

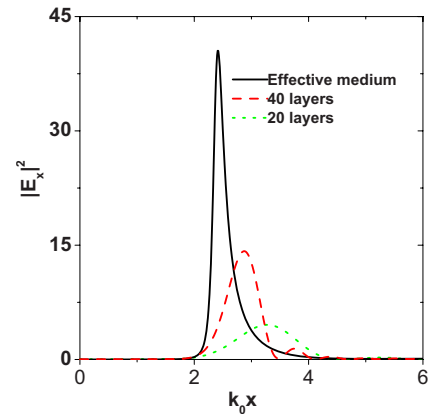


FIG. 6. (Color online) The transmitted field intensity for different layer numbers for effective medium case (black solid lines),  $n=40$  (red dashed lines), and  $n=20$  (green dotted lines). The relevant parameters are the same as those in Fig. 4.

structure, the resonance region was always excluded due to large absorption.<sup>14,15</sup> More recently, Arnold<sup>38</sup> reported that by controlling the amplitude and phase of the reflection, the quality of subwavelength near-field images can be significantly improved. To achieve the desired reflection, one may use plasmonic reflectors to require enhancement of the evanescent fields. Here, plasmonic reflectors may be replaced with reflectors made of metal-dielectric composite films, and many freedoms such as the particles' shape and the volume fraction can be adjusted.

#### ACKNOWLEDGMENTS

This work was supported by the National Natural Science Foundation of China under Grant No. 10674098, the National Basic Research Program under Grant No. 2004CB719801, and the Natural Science of Jiangsu Province under Grant No. BK2007046.

\*Corresponding author; leigao@suda.edu.cn

<sup>1</sup>J. B. Pendry, Phys. Rev. Lett. **85**, 3966 (2000).

<sup>2</sup>R. W. Ziolkowski and E. Heyman, Phys. Rev. E **64**, 056625 (2001).

<sup>3</sup>N. Fang, H. Lee, C. Sun, and X. Zhang, Science **308**, 534 (2005).

<sup>4</sup>D. O. Melville and R. J. Blaikie, Opt. Express **13**, 2127 (2005).

<sup>5</sup>S. A. Ramakrishna, J. B. Pendry, M. C. K. Wiltshire, and W. J. Stewart, J. Mod. Opt. **50**, 1419 (2003).

<sup>6</sup>C. J. Tang and L. Gao, J. Phys.: Condens. Matter **16**, 4743 (2004).

<sup>7</sup>P. A. Belov and Y. Hao, Phys. Rev. B **73**, 113110 (2006).

<sup>8</sup>X. Li, S. L. He, and Y. Jin, Phys. Rev. B **75**, 045103 (2007).

<sup>9</sup>K. J. Webb and M. Yang, Opt. Lett. **31**, 2130 (2006).

<sup>10</sup>B. Wood, J. B. Pendry, and D. P. Tsai, Phys. Rev. B **74**, 115116 (2006).

<sup>11</sup>D. O. S. Melville and R. J. Blaikie, J. Opt. Soc. Am. B **23**, 461

(2006).

<sup>12</sup>C. T. Wang, Y. H. Zhao, D. C. Gan, C. L. Du, and X. G. Luo, Opt. Express **16**, 4217 (2008).

<sup>13</sup>L. Gao and Y. Ma, Proc. SPIE **6328**, 63280G (2006).

<sup>14</sup>L. H. Shi, L. Gao, S. L. He, and B. W. Li, Phys. Rev. B **76**, 045116 (2007).

<sup>15</sup>W. S. Cai, D. A. Genov, and V. M. Shalaev, Phys. Rev. B **72**, 193101 (2005).

<sup>16</sup>G. X. Li, H. L. Tam, F. Y. Wang, and K. W. Cheah, J. Appl. Phys. **102**, 116101 (2007).

<sup>17</sup>A. I. Cabuz, D. Felbacq, and D. Cassagne, Phys. Rev. Lett. **98**, 037403 (2007).

<sup>18</sup>L. Gao, Phys. Rev. E **73**, 036602 (2006).

<sup>19</sup>D. Stroud, Phys. Rev. B **12**, 3368 (1975).

<sup>20</sup>J. W. Haus, R. Inguva, and C. M. Bowden, Phys. Rev. A **40**, 5729 (1989).

<sup>21</sup>J. S. Ahn, K. H. Kim, T. W. Noh, D. H. Riu, K. H. Boo, and H.

- E. Kim, Phys. Rev. B **52**, 15244 (1995).
- <sup>22</sup>T. K. Xia, P. M. Hui, and D. Stroud, J. Appl. Phys. **67**, 2736 (1990).
- <sup>23</sup>C. Y. You, S. C. Shin, and S. Y. Kim, Phys. Rev. B **55**, 5953 (1997).
- <sup>24</sup>S. Berthier J. Phys. I **4**, 303 (1994).
- <sup>25</sup>F. Brouers, J. P. Clerc, and G. Giraud, Phys. Rev. B **44**, 5299 (1991).
- <sup>26</sup>W. S. Weiglhofer, J. Phys. A **31**, 7191 (1998).
- <sup>27</sup>B. Michel and W. S. Weiglhofer, AEU, Int. J. Electron. Commun. **51**, 219 (1997).
- <sup>28</sup>T. G. Mackay, J. Phys. D **36**, 583 (2003).
- <sup>29</sup>T. G. Mackay and A. Lakhtakia, J. Opt. A, Pure Appl. Opt. **7**, 669 (2005).
- <sup>30</sup>S. M. Wang and L. Gao, Eur. Phys. J. B **48**, 29 (2005).
- <sup>31</sup>T. Dumelow, Jose Alzimir Pereira da Costa, and V. N. Freire, Phys. Rev. B **72**, 235115 (2005).
- <sup>32</sup>V. Yannopapas and A. Moroz, J. Phys.: Condens. Matter **17**, 3717 (2005).
- <sup>33</sup>V. Yannopapas, Appl. Phys. A: Mater. Sci. Process. **87**, 259 (2007).
- <sup>34</sup>P. B. Johnson and R. W. Christy, Phys. Rev. B **6**, 4370 (1972).
- <sup>35</sup>F. Zolla, D. Felbacq, and G. Bouchitte, Phys. Rev. E **74**, 056612 (2006).
- <sup>36</sup>G. Bouchitte and D. Felbacq, SIAM J. Appl. Math. **66**, 2061 (2006).
- <sup>37</sup>T. G. Mackay, J. Nanophotonics **1**, 019501 (2007).
- <sup>38</sup>M. D. Arnold and R. J. Blaikie, Opt. Express **15**, 11542 (2007).